



Article

Luminescent Behavior of Liquid–Crystalline Gold(I) Complexes Bearing a Carbazole Moiety: Effects of Substituent Bulkiness

Kumar Siddhant ¹, Ganesan Prabusankar ² and Osamu Tsutsumi ^{1,*}

¹ Department of Applied Chemistry, College of Life Sciences, Ritsumeikan University, Kusatsu 525-8577, Japan; gr0451pe@ed.ritsumei.ac.jp

² Department of Chemistry, Indian Institute of Technology Hyderabad, Kandi 502285, India; prabu@chy.iith.ac.in

* Correspondence: tsutsumi@sk.ritsumei.ac.jp

Abstract: Organometallic materials that exhibit white luminescence in condensed phases are of considerable interest for lighting and display applications. Herein, new carbazole-based Au(I) complexes containing an isocyanide group and a long pentyl chain were synthesized. The complex with an unsubstituted carbazole moiety exhibited a white emission at room temperature as well as nematic liquid crystalline behavior. Color tunability from white to blue was achieved when bulkier substituents were introduced at the 3 and 6 positions of the carbazole moiety. Furthermore, all complexes possessed long phosphorescence lifetimes in the crystal state. The proposed design framework provides new opportunities for practical applications using luminescent organometallic molecules.

Keywords: white emission; liquid crystal; aggregated structure; gold(I) complex; carbazole moiety



Citation: Siddhant, K.; Prabusankar, G.; Tsutsumi, O. Luminescent Behavior of Liquid–Crystalline Gold(I) Complexes Bearing a Carbazole Moiety: Effects of Substituent Bulkiness. *Crystals* **2022**, *12*, 810. <https://doi.org/10.3390/cryst12060810>

Academic Editor: Paul R. Raithby

Received: 12 May 2022

Accepted: 7 June 2022

Published: 8 June 2022

Publisher's Note: MDPI stays neutral with regard to jurisdictional claims in published maps and institutional affiliations.



Copyright: © 2022 by the authors. Licensee MDPI, Basel, Switzerland. This article is an open access article distributed under the terms and conditions of the Creative Commons Attribution (CC BY) license (<https://creativecommons.org/licenses/by/4.0/>).

1. Introduction

Luminescent molecules are of importance in both materials and life sciences [1–3]. In particular, white-light-emitting organometallic materials have attracted increasing attention owing to their potential applications in lighting devices and display media. However, the generation of white light commonly requires the simultaneous emission of the three primary RGB colors (red, green, and blue) or at least two complementary colors [4]. Moreover, achieving white room temperature phosphorescence (RTP) from a single molecule is highly challenging because the different radiation pathways involved in the emission process can affect each other [5].

Although most luminescent organometallic molecules exhibit efficient photoluminescence in dilute solutions, aggregation in condensed phases (e.g., crystals and solid films) typically results in partial or complete quenching of their luminescence. This phenomenon, known as aggregation-caused quenching (ACQ), is common in organometallic molecules with π -electron systems and prevents their practical use. Owing to the essential contribution of molecular aggregation to luminescence properties, aggregated structures play an important role in luminescence behavior [5–10]. Liquid crystals (LCs) are a unique class of soft materials that flow like liquids and possess a long-range orientational order similar to that of crystals [7,11–14]. LCs have the potential to control the aggregated structure of luminescent materials. Moreover, the material properties and aggregated structures of LC molecules can be influenced by various external stimuli. The molecular skeleton of an LC molecule generally consists of a rod-like rigid core and flexible chains, such as alkoxy and alkyl chains. Various aggregation-induced emission (AIE)-active LC systems have been developed [15,16].

Au(I) complexes show very interesting behavior because of their metallophilic d^{10} – d^{10} interactions. The emission observed in Au(I) complexes results from an interatomic Au–Au interaction; thus, Au(I) complexes exhibit the luminescence mainly from their aggregates

and have been known as the AIE-active material. The Au–Au interaction as well as the luminescence behavior can be tuned via not only modification of the chemical structure around Au atoms but also by controlling the aggregated structures [5]. For instance, previously synthesized Au(I) complexes with isocyanides and phenylacetylene ligands exhibited interesting AIE properties [16]. Furthermore, our group reported a biphenyl ring system with an LC phase, where luminescence was observed in both the crystal and LC phases [14].

Carbazole-based luminescent materials are valuable candidates for photoelectronic devices. Carbazole units are suitable building blocks for functional materials in organometallic light-emitting diodes because of their high triplet energy and good thermal stability [17]. Herein, we developed a carbazole-based Au(I) complex with a flexible pentyl isocyanide group. This complex shows a white emission at room temperature (rt) along with a nematic (N) LC phase. Color tunability from white (**Cbz-H**) to blue (**Cbz-*t*-Bu**) was also realized by changing the substituents at the 3 and 6 positions of the carbazole moiety.

2. Materials and Methods

2.1. Materials

Compound **1-R** was prepared by following the reported procedure [18]. Complexes **Cbz-H**, **Cbz-Br**, and **Cbz-*t*-Bu** were prepared via a one-step synthetic route using compounds **1-R**. The reagents and solvents used for the synthesis were obtained from commercial sources and used without further purification. ^1H and ^{13}C NMR spectra were recorded using a JEOL ECS-400 spectrometer (JEOL, Tokyo, Japan) (400 MHz for ^1H and 100 MHz for ^{13}C) in CDCl_3 (Figures S1–S3 for ^1H NMR, Figures S4–S6 for ^{13}C NMR). Chemical shifts are reported in parts per million (ppm), using the residual ^1H or ^{13}C in the NMR solvent as an internal reference. IR spectra were obtained using the KBr disk method with a FT/IR-4100 spectrometer (JASCO, Tokyo, Japan), and all spectra are reported in wavenumbers (cm^{-1}). Elemental analysis (C, H, and N) was performed using a Micro Corder JM10 analyzer (J-Science, Tokyo, Japan). Electrospray ionization mass spectrometry (ESI-MS) was carried out using a Bruker micrOTOF II instrument (JEOL, Tokyo, Japan).

2.1.1. Synthesis of Cbz-H

Compound **1-H** (0.30 g, 1.5 mmol) and (tht) AuCl (tht: tetrahydrothiophene) (0.47 g, 1.5 mmol) were dissolved in 10 mL of CH_2Cl_2 . Then, a methanol (10 mL) solution of CH_3COONa (0.61 g, 7.2 mmol) was added dropwise, and the resulting mixture was stirred for 2 h at rt. Subsequently, 1-pentyl isocyanide (0.071 g, 0.73 mmol) in CH_2Cl_2 (7 mL) was added and the mixture was stirred for a further 1 h at rt. The reaction mixture was then filtered through Celite and evaporated under vacuum. The crude product was purified by silica gel column chromatography using CH_2Cl_2 as the mobile phase and then recrystallized in a $\text{CH}_2\text{Cl}_2/n$ -hexane mixed solvent system (1:2, *v/v*) to obtain 0.28 g, 0.57 mmol of the title complex as white crystal in 78% yield, mp 156 °C. ^1H NMR (400 MHz, CDCl_3 , δ): 8.06–8.04 (d, $J = 7.5$ Hz, 2H, ArH), 7.56–7.54 (dd, $J = 7.5$ Hz, 2H, ArH), 7.44 (d, $J = 7.5$ Hz, 2H, ArH), 7.25–7.20 (m, $J = 7.5$ Hz, 2H, ArH), 5.15–5.12 (s, 2H, ArNCH), 3.52–3.49 (t, 2H, NCH), 1.73 (s, $J = 7.1$ Hz, 2H, CH_2), 1.36–1.2 (m, $J = 7.1$ Hz, 2H, CH_2), 0.95–0.87 (t, $J = 8$ Hz 3H, CH_3). ^{13}C NMR (400 MHz, CDCl_3 , δ): 140.04 (9-C in carbazole), 125.78 (2,7-C in carbazole), 123.09 (Au–C \equiv N), 120.23 (3,6-C in carbazole), 119.10 (4-C in carbazole), 114.84 (4-C in carbazole), 109.29 (1,8-C in carbazole), 77.13 (Au–C \equiv C), 43.83 (N– CH_2), 33.44 (N– CH_2 in carbazole), 28.22 (NCH $_2$ CH $_2$), 27.56 (NCH $_2$ CH $_2$ CH $_2$), 21.71 (CH $_2$ CH $_3$), 13.79 (CH $_2$ CH $_3$).

FTIR (KBr, cm^{-1}): 3049, 2953, 2248, 1460. ESI-MS m/z : $[\text{M} + \text{H}]^+$ calcd for $\text{C}_{21}\text{H}_{21}\text{AuN}_2$, 499.14; found, 499.11. Anal calcd for $\text{C}_{21}\text{H}_{21}\text{AuN}_2$: C, 50.61; H, 4.25; Au, 39.52; N, 5.62; found: C, 50.43; H, 4.12; N, 5.51.

2.1.2. Synthesis of Cbz-Br

The same procedure was followed using **1-Br** for the synthesis of **Cbz-Br** to obtain the title complex as a white solid in 84% yield, mp 168 °C. ^1H NMR (400 MHz, CDCl_3 , δ): 8.11–8.10 (d, $J = 7.5$ Hz, 2H, ArH), 7.56–7.53 (dd, $J = 7.5$ Hz, 2H, ArH), 7.44–7.42 (d, $J = 7.5$ Hz, 2H, ArH), 5.09 (s, 2H, ArNCH), 3.56–3.52 (s, 2H, NCH), 1.76 (s, $J = 7.1$ Hz, 2H, CH_2), 1.39–1.32 (m, $J = 7.1$ Hz, 2H, CH_2), 0.92–0.89 (t, $J = 8$ Hz 3H, CH_3). ^{13}C NMR (400 MHz, CDCl_3 , δ): 139.05 (9-C in carbazole), 129.13 (2,7-C in carbazole), 123.84 (Au–C \equiv N), 123.17 (3,6-C–Br in carbazole), 115.72 (4-C in carbazole), 112.34 (4-C in carbazole), 111.13 (1,8-C in carbazole), 77.11 (Au–C \equiv C), 40.01 (N– CH_2), 33.79 (N– CH_2 in carbazole), 33.41 (N CH_2CH_2), 27.77 (N $\text{CH}_2\text{CH}_2\text{CH}_2$), 21.75 (CH_2CH_3), 13.80 (CH_2CH_3). FTIR (KBr, cm^{-1}): 3073, 2957, 2245, 1472, 645. ESI-MS m/z : $[\text{M}]^+$ calcd for $\text{C}_{21}\text{H}_{19}\text{AuBr}_2\text{N}_2$, 653.96; found, 653.46. Anal calcd for $\text{C}_{21}\text{H}_{19}\text{AuBr}_2\text{N}_2$: C, 38.44; H, 2.92; Au, 30.02; N, 4.27; Br, 24.35 found: C, 38.27; H, 2.79; N, 4.21.

2.1.3. Synthesis of Cbz-*t*-Bu

The same procedure was followed using **1-*t*-Bu** for the synthesis of **Cbz-*t*-Bu** to obtain the title complex as white solid in 81% yield, mp 190 °C. ^1H NMR (400 MHz, CDCl_3 , δ): 8.04 (d, $J = 7.5$ Hz, 2H, ArH), 7.50–7.47 (t, $J = 7.5$ Hz, 2H, ArH), 7.45–7.42 (d, $J = 7.5$ Hz, 2H, ArH), 5.09 (s, 2H, ArNCH), 3.43–3.40 (t, 2H, NCH), 1.53 (s, $J = 7.1$ Hz, 2H, CH_2), 1.42 (s, 18H, CH_3), 1.29–1.28 (m, $J = 7.1$ Hz, 4H, CH_2), 0.87 (t, $J = 8$ Hz 3H, CH_3). ^{13}C NMR (400 MHz, CDCl_3 , δ): 141.72 (C(CH_3) $_3$), 138.60 (9-C in carbazole), 123.42 (Au–C \equiv N), 122.98 (2,7-C in carbazole), 116.17 (4-C in carbazole), 114.45 (4a-C in carbazole), 108.59 (1,8-C in carbazole), 77.12 (Au–C \equiv C), 43.86 (N– CH_2), 34.74 (N– CH_2 in carbazole), 33.41 (N CH_2CH_2), 32.16 (C(CH_3) $_3$), 27.61 (N $\text{CH}_2\text{CH}_2\text{CH}_2$), 21.729 (CH_2CH_3), 13.79 (CH_2CH_3). FTIR (KBr, cm^{-1}): 3044, 2953, 2245, 1477. ESI-MS m/z : $[\text{M} + \text{H}]^+$ calcd for $\text{C}_{29}\text{H}_{37}\text{AuN}_2$, 611.27; found, 611.26. Anal calcd for $\text{C}_{29}\text{H}_{37}\text{AuN}_2$: C, 57.05; H, 6.11; Au, 32.26; N, 4.59; found: C, 56.94; H, 6.05; N, 4.37.

2.2. X-ray Crystallography

A single crystal was prepared via slow evaporation in a mixed solvent system (CH_2Cl_2 /*n*-hexane). The obtained crystal was mounted on a glass fiber. The omega scanning technique was applied to collect the reflection data using a Bruker D8 goniometer (Bruker, Millerica, MA, USA) with monochromatized $\text{MoK}\alpha$ radiation ($\lambda = 0.71075$ Å). To estimate the actual crystal structure of the synthesized materials, measurements were performed at ambient temperature (296 K). The initial structure of the unit cell was determined via a direct method using APEX2. The structural model was refined by the full-matrix least-squares method using SHELXL-2014/6. All calculations were performed using the SHELXL software [19,20]. The crystallographic data for the synthesized compounds are summarized in the Supplementary Materials, and the indexed data were deposited in the Cambridge Crystallographic Data Centre (CCDC) database (CCDC 2160379 for **Cbz-H**). These data can be obtained free of charge via <http://www.ccdc.cam.ac.uk/conts/retrieving.html> accessed on 21 March 2022 (or from the CCDC, 12 Union Road, Cambridge CB2 1EZ, UK; Fax: +44-1223-336033; E-mail: deposit@ccdc.cam.ac.uk).

2.3. Phase Transition Behavior

LC behavior as well as the melting points of the complexes were observed via polarized optical microscopy (POM) using an Olympus BX51 (Tokyo, Japan) microscope equipped with a hot stage (Instec HCS302 hot stage with an mK1000 controller). To assess the thermochemical stability, thermogravimetric–differential thermal analysis (TG/DTA) was carried out using a DTG-60AH instrument (Shimadzu, Kyoto, Japan) at a heating rate of 5.0 °C min^{-1} in air. The thermodynamic parameters were determined via differential scanning calorimetry (DSC; SII X-DSC7000, Tokyo, Japan) at a scanning rate of 3.0 °C min^{-1} .

2.4. Photophysical Properties

UV–Vis absorption spectra were recorded on a JASCO V-550 (JASCO, Tokyo, Japan) absorption spectrometer, and steady-state photoluminescence spectra were recorded on a Hitachi F-7000 fluorescence spectrometer (Hitachi, Tokyo, Japan) with an R928 photomultiplier (Hamamatsu Photonics, Hamamatsu, Japan) as the detector. Photoluminescence lifetimes were measured at various excitation wavelengths using a Quantaaurus-Tau photoluminescence lifetime measurement system (C1136-21, Hamamatsu Photonics, Hamamatsu, Japan).

3. Results and Discussion

3.1. Synthesis and Characterization of Complex *Cbz-R*

Complex **Cbz-R** were synthesized according to the synthetic route shown in Figure 1. After purification, all complexes were characterized via ^1H NMR spectroscopy, mass spectrometry, and elemental analysis. All the analytical data (presented in the Materials and Methods section) confirmed that the desired products were obtained.

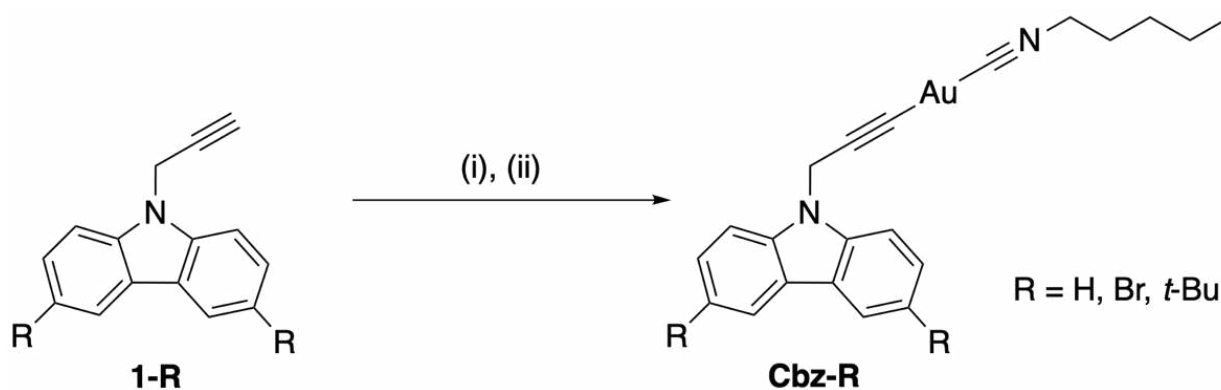


Figure 1. Molecular structure and synthetic route for complex **Cbz-R**: (i) (tht) AuCl/CH₂Cl₂, CH₃COONa/MeOH; (ii) 1-pentyl isocyanide.

Complex **Cbz-H** furnished single crystals suitable for X-ray crystallography via a slow evaporation technique using the mixed solvent system; however, suitable single crystals were not obtained for other complexes. To determine the molecular structure of **Cbz-H**, single-crystal X-ray diffraction (XRD) was performed at room temperature. The obtained crystal structure is shown in Figure 2. The corresponding crystallographic data and key structural parameters are summarized in Tables S1 and S2, respectively. According to the crystal structure, **Cbz-H** belongs to the triclinic space group $P\bar{1}$. The C1–Au–C2 bond angle is $\sim 180^\circ$ [21], and molecular packing gives a Au–Au bond distance of 6.4 Å, which suggests the absence of aurophilic interactions between the molecules. We have previously reported the structure of a similar Au(I) complex that has less-hindered 4-ethynylbiphenyl and alkyl isocyanide ligands [14]. This complex also crystallized in triclinic space group $P\bar{1}$, and the C1–Au–C2 bond angles were the same as in **Cbz-H**, i.e., $\sim 180^\circ$; however, the intermolecular Au–Au distance was 3.46 Å, which confirms the presence of intermolecular aurophilic interactions in the crystal. The longer intermolecular distance between Au atoms in **Cbz-H** is due to the bulkier carbazolylmethyl unit. Additionally, the face of the carbazole moiety is orthogonal to the C1–Au–C2 axis. We consider that this orthogonal structure of the bulky carbazole moiety resulted in the longer intermolecular Au–Au distance in the **Cbz-H** complex.

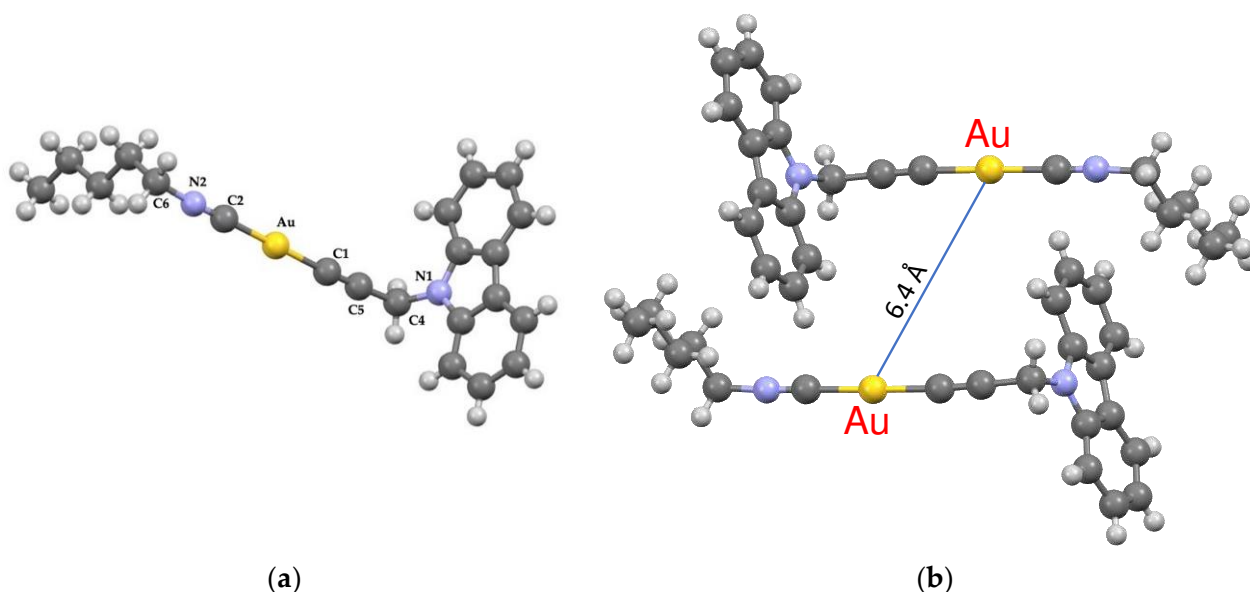


Figure 2. Molecular structure (a) and molecular packing structure (b) of complex **Cbz-H** determined via single-crystal X-ray diffraction at rt (gray, C; blue, N; yellow, Au; white, H).

3.2. Thermal Behavior of Complex **Cbz-R**

The thermal stability of complex **Cbz-R** was analyzed using TG/DTA measurements (Figure S7). The thermal decomposition temperature (T_{dec}) is defined as the temperature at which 5% weight loss occurs [22,23]. The TG/DTA thermograms show that all of the synthesized complexes are thermally stable up to 170–220 °C. The 12–15% weight loss observed near T_{dec} can be attributed to the loss of the isocyanide moieties. The second weight loss may be due to the removal of the propargyl moiety. The amount of residual ash obtained at 600 °C corresponds to the percentage of gold(I) in the complex.

The thermodynamic behavior was evaluated using DSC and POM techniques. The DSC thermogram of **Cbz-H** suggests LC behavior during heating (Figure S8). To further investigate this behavior, POM images were collected to examine the optical texture of **Cbz-H** (Figure 3). A schlieren texture was obtained at 93 °C, which confirmed that the observed phase for **Cbz-H** is the N phase [14,16]. In the DSC thermogram, a small endothermic peak was observed at 73 °C during the heating process, and an isotropic phase was achieved at 118 °C. The N phase was observed between these temperatures. However, in the cooling process of the DSC thermograms, no exothermic peak was observed. Through POM observation, we confirmed that the phase transition from the isotropic liquid to the amorphous solid occurred at ~80 °C, and that once **Cbz-H** was melted, the complex did not exhibit crystalline and LC phases.

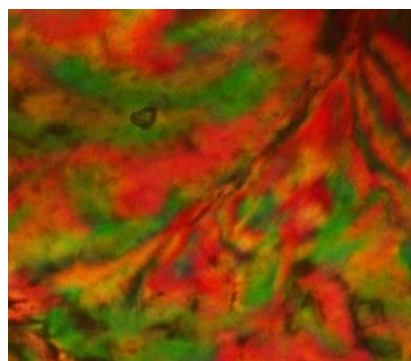


Figure 3. Optical texture of **Cbz-H** observed via polarized optical microscopy at 93 °C during the first heating process (scanning rate: 3.0 °C min⁻¹).

In contrast, no LC phases were observed for complexes **Cbz-Br** and **Cbz-*t*-Bu** at any temperature. In **Cbz-Br** and **Cbz-*t*-Bu**, the substituents attached at the 3 and 6 positions of the carbazole moiety are bulkier than H atoms (i.e., Br atoms or *t*-butyl groups). As the steric hindrance of these bulky substituents disturbs the LC alignment, only **Cbz-H** shows an LC phase [24–26].

3.3. Solution and Solid-State Photoluminescence Properties of Complex **Cbz-R**

The UV–vis absorption spectra of compounds **Cbz-H**, **Cbz-Br**, and **Cbz-*t*-Bu** were recorded in dilute CH₂Cl₂ solution. **Cbz-H** (2.1×10^{-5} mol L⁻¹), **Cbz-Br** (4.3×10^{-5} mol L⁻¹), and **Cbz-*t*-Bu** (3.3×10^{-5} mol L⁻¹) exhibited absorption bands at 293, 310, and 297 nm, respectively (Figure 4a), which may be attributable to a metal-to-ligand charge transfer (MLCT) transition or a ligand-based π - π^* transition [5,27,28]. All complexes also showed smaller absorption peaks with a vibronic structure at 340–360 nm. This small absorption band is known as the n - π^* transition of the carbazole unit. Additionally, it has also been reported that the absorption band at this wavelength originated from the transition from the alkynyl-to-isocyanide ligand-to-ligand charge transfer [29]. Thus, we can consider that both transitions are overlapped in this absorption band.

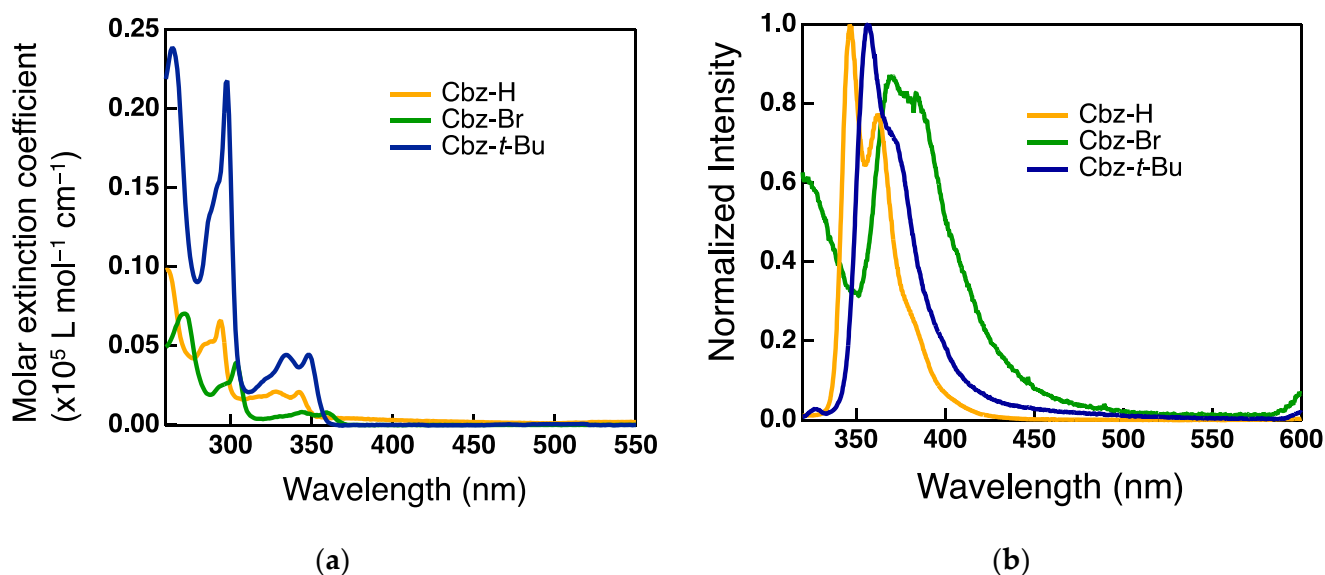


Figure 4. (a) UV–Vis absorption spectra of complex **Cbz-R** in CH₂Cl₂ solution: [**Cbz-H**], 2.1×10^{-5} mol L⁻¹; [**Cbz-Br**], 4.3×10^{-5} mol L⁻¹; [**Cbz-*t*-Bu**], 3.3×10^{-5} mol L⁻¹. (b) Normalized emission spectra of complex **Cbz-R** in CH₂Cl₂ solution: [**Cbz-H**], 2.1×10^{-5} mol L⁻¹, $\lambda_{\text{ex}} = 293$ nm; [**Cbz-Br**], 4.3×10^{-5} mol L⁻¹, $\lambda_{\text{ex}} = 300$ nm; [**Cbz-*t*-Bu**], 3.3×10^{-5} mol L⁻¹, $\lambda_{\text{ex}} = 297$ nm.

All complexes showed monomeric-type emissions with a vibronic structure at ~350 nm in dilute solutions (Figure 4b). Similar spectral shapes were observed at this wavelength in all complexes; however, in **Cbz-*t*-Bu** and **Cbz-Br**, the vibronic bands were slightly broadened. The emission peaks of **Cbz-H** and **Cbz-*t*-Bu** were observed at 375 and 380 nm, respectively, whereas that of **Cbz-Br** was slightly red-shifted to approximately 400 nm. Although the luminescence behaviors of all complexes were comparable in the dilute solution, significant differences were observed in the solid state.

The emission spectra of the complexes were obtained in the crystal state (Figure 5a). Each complex exhibited a peak in the region of 370–400 nm, which is similar to the emission peak in the solution state and can be considered a monomeric-type fluorescence emission. Furthermore, **Cbz-Br** and **Cbz-*t*-Bu** exhibited additional emission peaks at approximately 430 and 450 nm. Thus, the emission of these complexes in the crystal state is more structured than that in the crystal state and extends into the blue region. Furthermore, **Cbz-Br** exhibits a brighter blue emission than **Cbz-*t*-Bu** owing to the heavy-atom effect [30]. In

contrast, the emission of **Cbz-H** covers the entire spectral range, including a prominent peak at approximately 550 nm due to crystallization-induced phosphorescence [31–33]. Consequently, **Cbz-H** shows a white emission. As shown by the CIE plot (Figure 5b), **Cbz-H**, **Cbz-Br**, and **Cbz-*t*-Bu** show white, bluish-white, and bluish emissions, respectively. Thus, color tunability from white to blue was successfully achieved by changing the substituents at the 3 and 6 positions of the carbazole moiety. The color tunability of these complexes can be attributed to the introduction of bulky substituents, which inhibits free rotation of the luminophore.

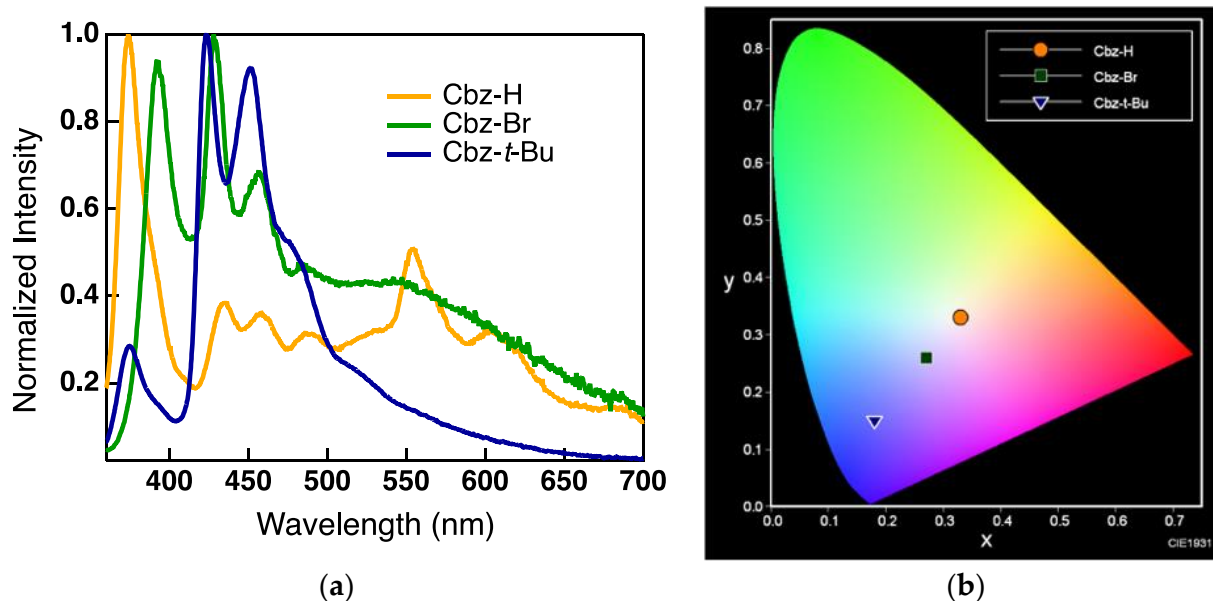


Figure 5. (a) Solid-state emission spectra ($\lambda_{\text{ex}} = 300$ nm) of complex **Cbz-R** (orange, **Cbz-H**; green, **Cbz-Br**; blue, **Cbz-*t*-Bu**). (b) CIE plot for the luminescence of complex **Cbz-R** in the crystal state.

To further clarify the photophysical properties of these complexes, the lifetimes and luminescence quantum yields were measured in the crystal state at room temperature (Figures S13–S15, Table S3). The decay profiles were well-fitted using a biexponential function. In all complexes, it was confirmed that the emission band at <400 nm was fluorescence due to the S_1-S_0 transition. In **Cbz-H**, the emission at 450 nm decayed on a nanosecond timescale, indicating that the emission bands in this wavelength region can be also assigned to fluorescence emitted from a higher excited state (S_n). In contrast, the emission at 550 nm contains a component with a lifetime of the microsecond timescale, suggesting that a part of this band can be attributed to phosphorescence. Interestingly, in **Cbz-Br**, emissions at 450 nm and 550 nm decayed on a microsecond timescale, and both emission bands can be attributed to phosphorescence due to the heavy-atom effects of the Br atoms. In **Cbz-*t*-Bu**, contrary to **Cbz-H**, phosphorescence was observed at 450 nm; however, fluorescence mainly contributed to the emission at 550 nm. In the **Cbz-*t*-Bu** crystal, we consider that phosphorescence from monomers of the complex was observed at 450 nm, and that fluorescence from the aggregates, i.e., excimer-type fluorescence, was observed at ~550 nm.

As shown in Table S3, the complexes had luminescence quantum yields (Φ) of 0.34–2.3% in the crystal state, even at room temperature in air. The excitation spectra of the crystals (Figure S9) revealed an excitation band at shorter wavelengths (320–340 nm), which is assigned to the S_0-S_n transition. The excitation spectra of all complexes showed an additional band at longer wavelengths (380–430 nm). We previously reported that similar Au(I) complexes with ethynyl and isocyanide ligands showed an efficient direct S_0-T_n transition owing to aggregation; that is, the S_0-T_n transition is enhanced by not only the heavy-atom effect but also the aggregation of Au(I) complexes. Thus, we conclude that the

longer-wavelength band in the excitation spectra can be assigned to a spin-forbidden direct S_0-T_n transition. Because the spin-forbidden transition occurs efficiently, the complexes show intense RTP in crystals under ambient conditions [14,34].

The photoluminescence of **Cbz-H** in the LC phase was also examined to determine the effects of the phase structure on luminescence behavior (Figure S10). The emission intensity levels were recorded at various temperatures. The emission intensity gradually decreased upon heating from rt to the LC phase, which indicates that a nonradiative decay was promoted by thermal motion of the Au(I) complex [14,16,22]. The emission intensity was recovered in the cooling process; however, it still remained lower than that of the original crystal before heating. This behavior is attributed to the crystal size dependence of the aggregation-enhanced spin-forbidden transition [14,34].

To obtain further insight into the luminescence properties, photophysical studies were performed in a mixed water–tetrahydrofuran (THF) system with various volume fractions of water. As all compounds showed good solubility in THF and very poor solubility in water, increasing the volume fraction of water induced aggregation. As shown in Figure S11, when the water concentration increased, the luminescence intensity decreased because of molecular aggregation. These results demonstrate that complexes of **Cbz-R** exhibit ACQ behavior [7]. In the case of **Cbz-H**, the same spectral shape was observed in the mixed solvent with a high water fraction as that in pure THF; namely, the spectral shape of aggregates in the mixed solvent was different from those in the crystal and LC, as shown in Figure S10. The results suggest that **Cbz-H** formed aggregates with different aggregate structures from the crystal, and that the luminescence behavior of this complex is sensitive to its aggregated structure, although no change in the spectral shape was observed via crystal-to-LC phase transition.

4. Conclusions

Color tunability was observed for carbazole-based Au(I) complexes, with a color change from white to blue occurring as the steric bulkiness of the carbazole moiety increased. Furthermore, all complexes showed phosphorescence in the crystal state. Notably, complex **Cbz-H** showed an N phase along with a white emission at room temperature. However, no LC phases were observed for **Cbz-Br** and **Cbz-*t*-Bu**. These findings suggest a new approach for designing luminescent materials.

Supplementary Materials: The following are available online at <https://www.mdpi.com/article/10.3390/cryst12060810/s1>: Figure S1: ^1H NMR spectra of complex **Cbz-H**. Figure S2: ^1H NMR spectra of complex **Cbz-Br**. Figure S3: ^1H NMR spectra of complex **Cbz-*t*-Bu**. Figure S4: ^{13}C NMR spectra of complex **Cbz-H**. Figure S5: ^{13}C NMR spectra of complex **Cbz-Br**. Figure S6: ^{13}C NMR spectra of complex **Cbz-*t*-Bu**. Table S1: Crystallographic data of complex **Cbz-H**. Table S2: Optimized bond parameters for **Cbz-H**. Figure S7: TG/DTA thermograms of complex **Cbz-R**. Figure S8: DSC thermogram of complex **Cbz-H**. Table S3: Photoluminescence decay parameters of complex **Cbz-R**. Figure S9: Excitation spectra of complex **Cbz-R** in solid state. Figure S10: Solid-state emission spectra of complex **Cbz-H** after first heating and cooling. Figure S11: Emission spectra of complex **Cbz-R** in THF–water mixture. Figure S12: Emission spectra of complex **Cbz-R** in CH_2Cl_2 before and after degassing. Figures S13–S15: Photoluminescence decay profile of complex **Cbz-R**.

Author Contributions: Conceptualization, O.T. and G.P.; methodology, K.S.; formal analysis, K.S.; investigation, K.S.; writing—original draft preparation, K.S.; writing—review and editing, O.T. and G.P.; supervision, O.T. and G.P.; project administration, O.T.; funding acquisition, O.T. All authors have read and agreed to the published version of the manuscript.

Funding: This research was supported by the Japan-India Science Cooperative Program between JSPS and DST (JPJSBP120217715), JICA, and the Cooperative Research Program of the Network Joint Research Centre for Materials and Devices.

Institutional Review Board Statement: Not applicable.

Informed Consent Statement: Not applicable.

Data Availability Statement: The data presented in this study are available in the article and Supplementary Materials.

Conflicts of Interest: The authors declare no conflict of interest.

References

1. Ghosh, B.; Shirahata, N. Colloidal silicon quantum dots: Synthesis and luminescence tuning from the near-UV to the near-IR range. *Sci. Technol. Adv. Mater.* **2014**, *15*, 014207. [[CrossRef](#)] [[PubMed](#)]
2. Dubey, V.; Som, S.; Kumar, V. (Eds.) *Luminescent Materials in Display and Biomedical Applications*, 1st ed.; CRC Press: Boca Raton, FL, USA, 2020.
3. Shizu, K.; Lee, J.; Tanaka, H.; Nomura, H.; Yasuda, T.; Kaji, H.; Adachi, C. Highly efficient electroluminescence from purely organic donor–acceptor systems. *Pure Appl. Chem.* **2015**, *87*, 627–638. [[CrossRef](#)]
4. Li, D.; Hu, W.; Wang, J.; Zhang, Q.; Cao, X.-M.; Ma, X.; Tian, H. White-light emission from a single organic compound with unique self-folded conformation and multistimuli responsiveness. *Chem. Sci.* **2018**, *9*, 5709–5715. [[CrossRef](#)] [[PubMed](#)]
5. Sathyanarayana, A.; Siddhant, K.; Yamane, M.; Hisano, K.; Prabusankar, G.; Tsutsumi, O. Tuning the Au–Au interactions by varying the degree of polymerization in linear polymeric Au(I) N-heterocyclic carbene complexes. *J. Mater. Chem. C* **2022**, *10*, 6050–6060. [[CrossRef](#)]
6. Birks, J.B. *Photophysics of Aromatic Molecules*; Wiley-Interscience: London, UK, 1970.
7. Sami, H.; Younis, O.; Maruoka, Y.; Yamaguchi, K.; Siddhant, K.; Hisano, K.; Tsutsumi, O. Negative thermal quenching of photoluminescence from liquid-crystalline molecules in condensed phases. *Crystals* **2021**, *11*, 1555. [[CrossRef](#)]
8. Ronda, C.R. Emission and excitation mechanisms of phosphors. In *Luminescence: From Theory to Applications*; Ronda, C.R., Ed.; Wiley-VCH: Weinheim, Germany, 2008; pp. 1–34.
9. Xu, J.; Chua, M.H.; Tang, B.Z. (Eds.) *Aggregation-Induced Emission (AIE): A Practical Guide (Materials Today)*, 1st ed.; Elsevier: Amsterdam, The Netherlands, 2022.
10. Tang, Y.; Tang, B.Z. (Eds.) *Handbook of Aggregation-Induced Emission, Vol. 1: Tutorial Lectures and Mechanism Studies*; Wiley: Chichester, UK, 2022.
11. Khoo, I.-C. *Liquid Crystals*, 2nd ed.; Wiley Interscience: Hoboken, NJ, USA, 2007.
12. Schadt, M. Liquid crystal materials and liquid crystal displays. *Annu. Rev. Mater. Sci.* **1997**, *27*, 305–379. [[CrossRef](#)]
13. Demus, D.; Goodby, J.; Gray, G.W.; Spiess, H.-W.; Vill, V. (Eds.) *Handbook of Liquid Crystals*; Wiley-VCH: Weinheim, Germany, 1998.
14. Furoida, A.; Daitani, M.; Hisano, K.; Tsutsumi, O. Aggregation-enhanced room-temperature phosphorescence from Au(I) complexes bearing mesogenic biphenylethynyl ligands. *Molecules* **2021**, *26*, 7255. [[CrossRef](#)]
15. Yamada, S.; Rokusha, Y.; Kawano, R.; Fujisawa, K.; Tsutsumi, O. Mesogenic gold complexes showing aggregation-induced enhancement of phosphorescence in both crystalline and liquid-crystalline phases. *Faraday Discuss.* **2017**, *196*, 269–283. [[CrossRef](#)]
16. Fujisawa, K.; Kawakami, N.; Onishi, Y.; Izumi, Y.; Tamai, S.; Sugimoto, N.; Tsutsumi, O. Photoluminescent properties of liquid crystalline gold(I) isocyanide complexes with a rod-like molecular structure. *J. Mater. Chem. C* **2013**, *1*, 5359–5366. [[CrossRef](#)]
17. Chen, Z.; Liu, G.; Pu, S.; Liu, S.H. Carbazole-based aggregation-induced emission (AIE)-active gold(I) complex: Persistent room-temperature phosphorescence, reversible mechanochromism and vapochromism characteristics. *Dyes Pigm.* **2017**, *143*, 409–415. [[CrossRef](#)]
18. Taranekar, P.; Fulghum, T.; Patton, D.; Ponnampati, R.; Clyde, G.; Advincula, R. Investigating carbazole jacketed precursor dendrimers: Sonochemical synthesis, characterization and electrochemical cross-linking properties. *J. Am. Chem. Soc.* **2007**, *129*, 12537–12548. [[CrossRef](#)] [[PubMed](#)]
19. Sheldrick, G.M. Crystal structure refinement with SHELXL. *Acta Crystallogr. C* **2015**, *71*, 3–8. [[CrossRef](#)] [[PubMed](#)]
20. Sheldrick, G.M. A short history of SHELX. *Acta Crystallogr. A* **2008**, *64*, 112–122. [[CrossRef](#)] [[PubMed](#)]
21. Olmstead, M.M.; Jiang, F.; Attar, S.; Balch, A.L. Alteration of the aurophilic interactions in trimeric gold(I) compounds through charge transfer. Behavior of solvoluminescent Au₃(MeN=COMe)₃ in the presence of electron acceptors. *J. Am. Chem. Soc.* **2001**, *123*, 3260–3267. [[CrossRef](#)]
22. Fujisawa, K.; Okuda, Y.; Izumi, Y.; Nagamatsu, A.; Rokusha, Y.; Sadaike, Y.; Tsutsumi, O. Reversible thermal-mode control of luminescence from liquid-crystalline gold(I) complexes. *J. Mater. Chem. C* **2014**, *2*, 3549–3555. [[CrossRef](#)]
23. Kuroda, Y.; Nakamura, S.; Srinivas, K.; Sathyanarayana, A.; Prabusankar, G.; Hisano, K.; Tsutsumi, O. Thermochemically stable liquid-crystalline gold(I) complexes showing enhanced room temperature phosphorescence. *Crystals* **2019**, *9*, 227. [[CrossRef](#)]
24. Yamada, S.; Miyano, K.; Konno, T.; Agou, T.; Kubota, T.; Hosokai, T. Fluorine-containing bistolanes as light-emitting liquid crystalline molecules. *Org. Biomol. Chem.* **2017**, *15*, 5949–5958. [[CrossRef](#)]
25. Jamain, Z.; Omar, N.F.; Khairuddean, M. Synthesis and determination of thermotropic liquid crystalline behavior of cinnamaldehyde-based molecules with two Schiff base linking units. *Molecules* **2020**, *25*, 3780. [[CrossRef](#)]
26. Hu, G.; Kitney, S.P.; Liu, Y.; Zhang, K. Synthesis and mesomorphic behavior of novel (bisthiophene)benzene carbazole nematic liquid crystals. *Mol. Cryst. Liq. Cryst.* **2021**, *723*, 81–92. [[CrossRef](#)]
27. Ge, Z.; Hayakawa, T.; Ando, S.; Ueda, M.; Akiike, T.; Miyamoto, H.; Kajita, T.; Kakimoto, M. Spin-coated highly efficient phosphorescent organic light-emitting diodes based on bipolar triphenylamine-benzimidazole derivatives. *Adv. Funct. Mater.* **2008**, *18*, 584–590. [[CrossRef](#)]

28. Tang, M.-C.; Tsang, D.P.-K.; Wong, Y.-C.; Chan, M.-Y.; Wong, K.M.-C.; Yam, V.W.-W. Bipolar gold(III) complexes for solution-processable organic light-emitting devices with a small efficiency roll-off. *J. Am. Chem. Soc.* **2014**, *136*, 17861–17868. [[CrossRef](#)] [[PubMed](#)]
29. He, X.; Lam, W.H.; Zhu, N.; Yam, V.W.-W. Design and synthesis of calixarene-based bis-alkynyl-bridged dinuclear Au^I isonitrile complexes as luminescent ion probes by modulation of Au–Au interactions. *Chem. Eur. J.* **2009**, *15*, 8842–8851. [[CrossRef](#)] [[PubMed](#)]
30. Xu, P.; Qiu, Q.; Ye, X.; Wei, M.; Xi, W.; Feng, H.; Qian, Z. Halogenated tetraphenylethene with enhanced aggregation-induced emission: An anomalous anti-heavy-atom effect and self-reversible mechanochromism. *Chem. Commun.* **2019**, *55*, 14938–14941. [[CrossRef](#)] [[PubMed](#)]
31. Bi, X.; Shi, Y.; Peng, T.; Yue, S.; Wang, F.; Zheng, L.; Cao, Q.-E. Multi-stimuli responsive and multicolor adjustable pure organic room temperature fluorescence-phosphorescent dual-emission materials. *Adv. Funct. Mater.* **2021**, *31*, 2101312. [[CrossRef](#)]
32. Favereau, L.; Quinton, C.; Poriel, C.; Roisnel, T.; Jacquemin, D.; Crassous, J. Persistent organic room-temperature phosphorescence in cyclohexane-*trans*-1,2-bisphthalimide derivatives: The dramatic impact of heterochiral vs. homochiral interactions. *J. Phys. Chem. Lett.* **2020**, *11*, 6426–6434. [[CrossRef](#)] [[PubMed](#)]
33. Tsutsumi, O.; Tamaru, M.; Nakasato, H.; Shimai, S.; Panthai, S.; Kuroda, Y.; Yamaguchi, K.; Fujisawa, K.; Hisano, K. Highly efficient aggregation-induced room-temperature phosphorescence with extremely large Stokes shift emitted from trinuclear gold(I) complex crystals. *Molecules* **2019**, *24*, 4606. [[CrossRef](#)]
34. Ando, A.; Ozaki, K.; Shiina, U.; Nagao, E.; Hisano, K.; Kamada, K.; Tsutsumi, O. Aggregation-enhanced direct S₀–T_n transitions and room-temperature phosphorescence in gold(I)-complex single crystals. *Aggregate* **2022**, *3*, e125. [[CrossRef](#)]